23rd ABCM International Congress of Mechanical Engineering
December 6-11, 2015, Rio de Janeiro, RJ, Brazil

A NUMERICAL INVESTIGATION OF THE 14-XB FOREBODY LEADING-EDGE BLUNTNESS EFFECTS ON THE EXTERNAL AIRFLOW OF THE SCRAMJET INTAKE

João Vitor Marques Brito de Siqueira[1]
Maurício Antoniazzi Pinheiro Rosa[2]
[1]Instituto Tecnológico de Aeronáutica, São josé dos Campos, São Paulo
[2]Instituto de Estudos Avançados, São José dos Campos, São Paulo
Joaovitormarques22@hotmail.com
pinheiro@ieav.cta.br

Abstract. *The Institute for Advanced Studies (IEAv), at the Aerothermodynamics and Hypersonics Division (EAH), has been doing a series of studies with the purpose of developing a hypersonic prototype vehicle powered by a scramjet engine. In this way, numerical simulations have been performed to analyze the hypersonic flow over the inlet of the present vehicle configuration (14-XB) of the 14-X hypersonic vehicle prototype. The objective of this paper was analyzing the influence of the leading edge bluntness, as well as the use of different viscous models, on the formation of the boundary-layer and its interactions with the shock waves from the compression ramp and flow separation that usually occurs there. At first, it has been done an analysis of the influence of the leading-edge bluntness and the use of different viscous models on a hypersonic flow passing over a 9° single wedge and the interaction between the entropy layer and the boundary layer. Secondly, it has been done a validation analysis of the numerical viscous models used for calculating hypersonic flow over a double wedge with blunt leading edge through comparison with experimental data from the literature which has shown that the transitional flow models analyzed yield good results. At last, a numerical study was done for the inlet compression ramps of the 14-XB vehicle. For all analysis, it has been considered different leading edge sizes, wall thermal conditions and viscous flow modeling. Similarly to the sharp leading edge case, the separation bubble increase with wall temperature. Regarding the blunt leading edge size effect on the bubble size, it reaches a maximum at a certain edge radius and then decreases as the radius is further increased.*

Keywords: *leading-edge bluntness, scramjet inlet, flow separation, hypersonic flow, numerical simulation.*

1. INTRODUCTION

The Institute for Advanced Studies (IEAv), at the Aerothermodynamics and Hypersonic Division (EAH), is conducting a series of studies for developing a hypersonic prototype vehicle powered by a scramjet engine. The scramjet (supersonic combustion ramjet) is a variant of the ramjet air breathing propulsion engine. The difference is that in the scramjet combustion process the incoming compressed air is supersonic whereas the incoming compressed air is subsonic in the ramjet combustion process. The scramjet is composed of three main parts: converging inlet, where the incoming air is decelerated and compressed; combustor, where fuel is burned with oxygen to produce heat; and divergent nozzle, where the air, heated in the combustor, is accelerated to produce thrust (Anderson, 1989).

The design of the scramjet inlet is extremely important once its performance usually determines the engine overall performance (Anderson, 1989). The corners between the inlet compression ramps enable shock wave/boundary layer interactions (SWBLI) that may cause flow separation which alters considerably the flow field structure. Flow separation increases local thermal and mechanical loads which reduces the overall engine performance, may adversely affect the air flow properties at the combustor entrance and can even lead to more severe condition of engine unstart. As hypersonic vehicles should always have leading edges with some degree of bluntness in order to reduce heat flux at stagnant regions, it is very important to develop suitable methods and models for numerical simulations as well as to understand its effects on the intake airflow structure and operation.

Continuing the numerical studies on the development of a scramjet intake for the 14-X hypersonic vehicle, which have begun with a study of the 14XB configuration with forebody and cowl sharp leading edges. (Moura, 2014), this work extends this study to investigate the influence of leading edge bluntness. Laminar and two transitional flow models have been used to study the airflow structure which includes flow separation due to SWBLI. At first, it has been done an analysis of the influence of the leading-edge bluntness on the boundary-layer formation over a 9° single wedge and on the interaction between the entropy layer, formed behind the bowl shock wave of the blunt edge, and the boundary layer. Secondly, it has been done a validation analysis of the numerical viscous models used for calculating hypersonic flow over a double wedge with blunt leading edge through comparison with experimental data from the literature which has shown that the transitional flow models analyzed yield suitable results. And the last analysis performed in this work corresponds to the flow in the external part of the 14X-B intake. The results have confirmed previous observations (Neuenhahn and Olivier, 2006; Holden, 1971) that the separation region reaches a maximum length at a certain edge radius and then decreases as the radius is further increased**.**.

All numerical simulations were done with the ANSYS Fluent code and the viscous models available in it.

2. METHODOLOGY

In order to calculate numerically the airflow with the ANSYS Fluent (Ansys, 2014), the Reynolds-Averaged Navier-Stokes (RANS) equations of continuity Eq. (1), momentum conservation Eq. (2) and energy conservation Eq. (3) are used in the form presented below. Also, to close the system of equations, considering air as a calorically perfect gas, state equations for energy, enthalpy and the perfect gas law are considered, such that:

$$\frac{\partial \rho}{\partial t} + \nabla \cdot (\rho \vec{v}) = O \quad (1)$$

$$\frac{\partial}{\partial t}(\rho \vec{v}) + \nabla \cdot (\rho \vec{v}\vec{v}) = -\nabla p + \nabla \cdot \left(\bar{\bar{\tau}}_{eff}\right) \quad (2)$$

$$\frac{\partial}{\partial t}(\rho E) + \nabla \cdot [\vec{v}(\rho E + p)] = \nabla \cdot \left[k_{eff} \nabla T + \left(\bar{\bar{\tau}}_{eff} \cdot \vec{v}\right)\right] + S_h \quad (3)$$

$$E = h - \frac{P}{\rho} + \frac{v^2}{2} \quad (4)$$

$$dh = c_p\, dT \quad (5)$$

$$p = \rho RT \quad (6)$$

where ρ is density, $\vec{V}$ is velocity vector, p is static pressure, E is total energy, k is thermal conductivity, T is temperature, h is enthalpy, c_p is specific heat at constant pressure and R is the gas constant. The effective viscous stress tensor, $\bar{\bar{\tau}}_{eff}$, is given by:

$$\bar{\bar{\tau}}_{eff} = \mu_{eff} \left[(\nabla . \vec{v} + \nabla . \vec{v}^T) - \frac{2}{3} \nabla \ . \ \vec{v} I\right] \quad (7)$$

where I is the unit tensor and μ is the viscosity. The second term on the right-hand side represents the effect of volume dilation. The subscript in Eq. (3) means effective values, which adds the turbulent term whenever a turbulent model is in use.

The models used were those available in Fluent code for laminar flow, transitional flow with the *k-kl-ω* and Transition SST models, which will be covered briefly here. Transitional flow models have been used here because they should be able to capture the transition from laminar to turbulent flow that might occur in case of boundary-layer separation (Reinartz et al, 2007; Arnal and Délery, 2008; Moura, 2014). The Shear Stress Transport (SST) *k-ω* blends the accurate formulation of the standard *k-ω* with the *k-ε* formulation, which is more adequate for the free stream region (Menter, 1994). The *k-kl-ω* transitional flow model adds a third equation to the turbulent *k-ω* model, which predicts low-frequency velocity fluctuations in the laminar boundary-layer, which are precursors to transition (Walters and Cokljat, 2008). And the Transition SST model is a modification of the SST *k-ω*, coupling it with two more transport equations, one for intermittency and another for the transition onset criteria (Menter *et al*., 2006).

2.1. Computational domain and mesh

It has been created three different domains for the analyses presented in this work: one for a 9° single wedge, another one for the double wedge used for model validation and one last domain that correspond to the external compression geometry of the intake of the 14X-B vehicle. Once the aim of this work is to investigate the affects of leading-edge bluntness, in comparison to the sharp one, on the boundary layer formation and its interactions with the entropy layer and shock waves, it was necessary to create two different computational domains: one for blunt and another for sharp leading edge . Figure 1 shows the computational domains and meshes for the numerical calculations of a sharp (Fig. 1.a) and a blunt (Fig. 1.b) leading edge double wedge. Also in this figure, are presented the boundary conditions for the problem. As can be noted in this figure, it was chosen to present the results by rotating the whole geometry by the angle, Θ, of the first wedge, therefore the free stream flow direction presents the same angle with respect to the first wedge. Details of the free stream and geometry for the three analyses presented here can be obtained in Tab. 1 accordinly to Fig. 1.

Although not presented here, an extensive meshing analysis has been performed, for all cases analyzed in this work, by varying mesh sizing on the blunt leading edges and on the wedges, taking care to condense appropriately the mesh near the walls to capture adequately the boundary layer and the phenomena that occur there.

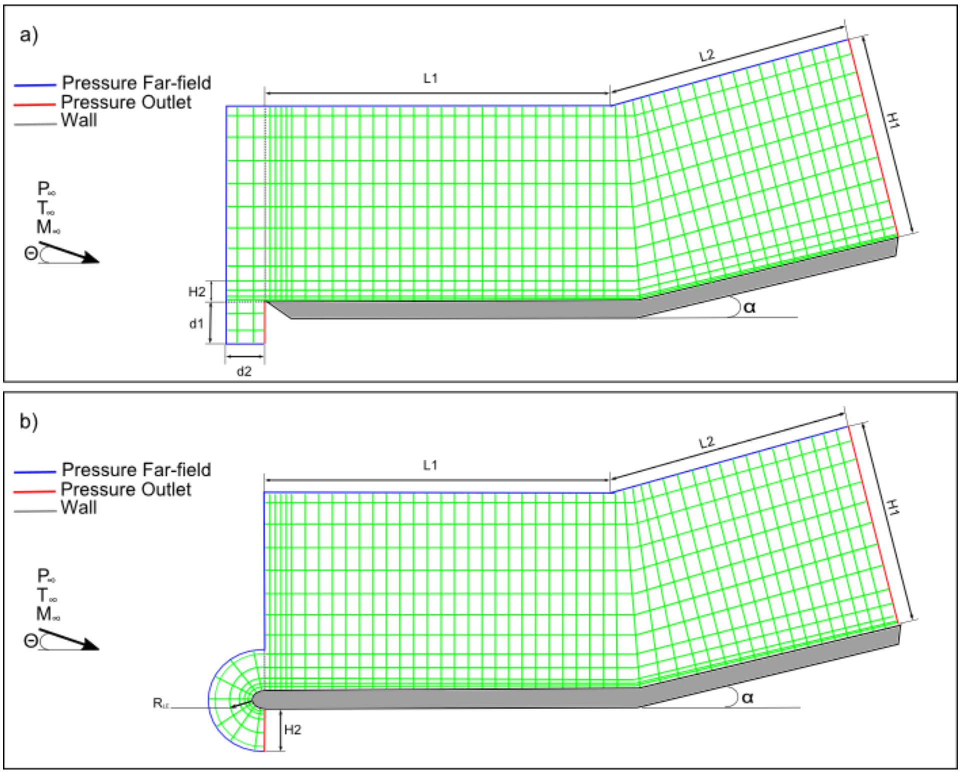

Figure 1. Computational domain and mesh of a double wedge with: a) sharp leading edge, and b) blunt leading edge.

Table 1. Freestream flow and wall conditions for the analyses.

Geometry	M_∞	ρ_∞ [Kg/m^3]	P_∞ [Pa]	T_∞ [K]	Θ [°]	Tw [K]
single wedge	8.1	0.0171	520	106	9	300 / 760
double wedge	8.1	0.0171	520	106	9	300 / 760
14X-B	7	0.018	1172	226.65	5.5	Adiabatic / 300

Table 2. Dimensions of the computational domains.

Geometry	L1 [mm]	L2 [mm]	H1 [mm]	α [°]
single wedge	140	-	60	-
double wedge	180	180	60	11.5
14X-B	660	351.18	120	14.5

3. RESULTS

3.1 – Single wedge analysis

In this subsection it is investigated the influence of the leading edge on the flow over a 9° single wedge. The free stream and wall thermal condition are the ones for both cases presented in Tab. 1 and the computational domain is presented in Tab. 2. Fig. 2 shows the Mach number contours near the leading edge for both sharp and 1 mm-radius blunt wedge. As can be seen in this figure, differently from the sharp edge result, the blunt edge generates a bowl shock around the leading edge which produces an entropy layer that interacts with a thinner boundary-layer along the wedge. The effects are to produce a wider and somewhat stronger shock wave and a thicker boundary layer develops downstream than for the sharp leading edge case. All these may affect considerably the flow downstream and also possible flow separation due to SWBLI near the corner with a compression wedge.

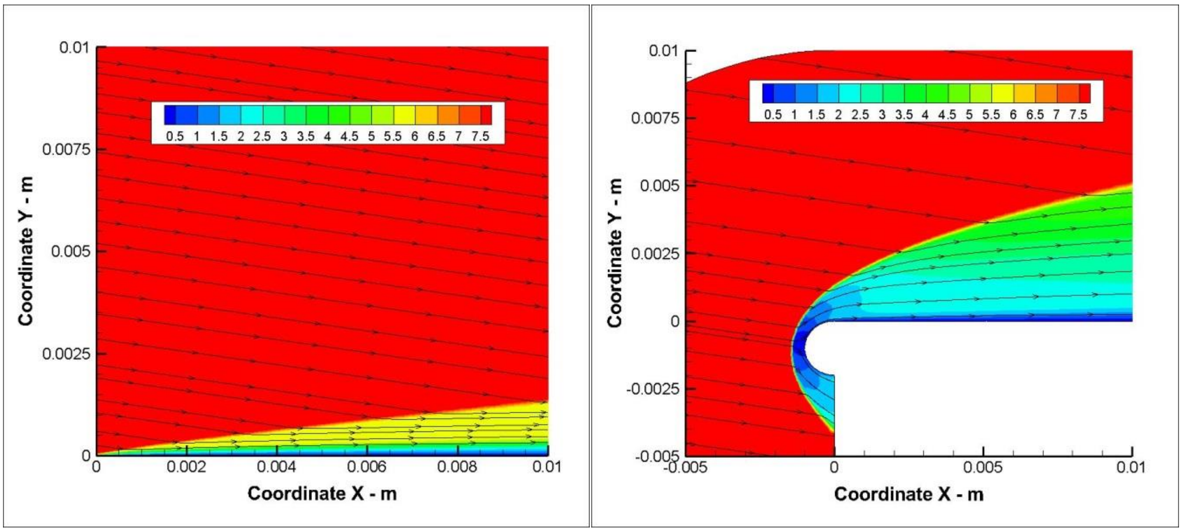

Figure 2. Mach number contours with streamlines for sharp leading edge (left) and blunt leading edge (right).

Figure 3 (left) shows the temperature profiles, orthogonal to the wall, at 120 mm distant from the leading edge cross-section, for different leading edge radii. As can be seen, both shock wave and boundary layers thicken due to the thicker entropy layer produced as the leading-edge radius increases.

Yet the heat flux over the leading edge has been analyzed. A hypersonic flow carries a lot of energy and when it hits the leading edge this energy is dissipated and there is a huge heat flux over the leading edge which may lead to very high structure temperatures and can seriously damage the vehicle. Laminar viscous model has been used in the analysis of the heat flux on the blunt leading edge. Figure 3 (right) shows the Stanton number on the leading edge as function of the edge radius and the imposed wall temperature. About 35% reduction in the Stanton number is achieved by increasing the edge radius from 0.5 to 1.0 millimeter. Therefore, in the aerothermodynamics design of hypersonic vehicles there is always a compromising between reducing surface heat flux without increasing significantly drag due to leading edge bluntness.

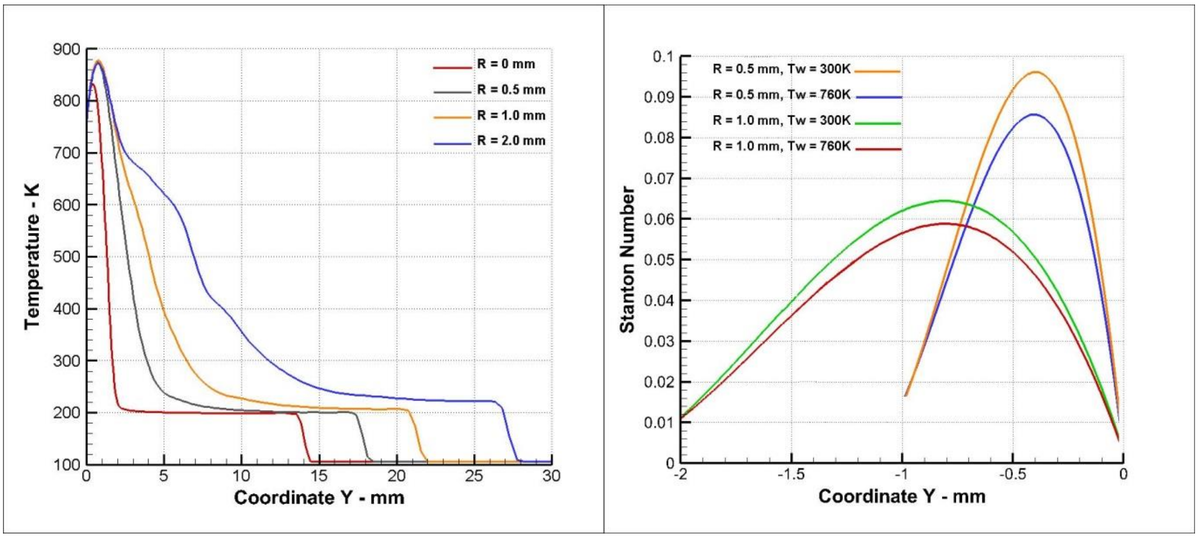

Figure 3. Temperature distributions at 120 mm distance from the leading edge cross-section (left) and Stanton number on the leading edge for different radii and wall temperature (right).

3.2 – Double wedge analysis and validation

This subsection has the purpose of validating the numerical methods and models through comparison with experimental data taken from the literature (Neuenhahn and Olivier, 2006). The geometry used in this reference is a double wedge with both sharp and blunt leading edge (see Tab. 1 and Tab. 2). In this analysis, both transitional flow models available in the Fluent code, the transition SST and the *k-kl-ω*, have been used. With the purpose of investigating the shock-wave interaction with the boundary layer (SWBLI) in the region of the double wedge intersection, Neuenhahn and Olivier (2006) measured the pressure and heat flux of a hypersonic flow over the wedges considering different wall temperatures and leading edge radii. Fig. 5 and 6 show the measured and calculated pressure coefficients over the wedges for both sharp and 1.0 mm-radius leading edge. Two wall temperature conditions were considered in this analysis: 300 K wall temperature for sharp leading edge, 300K and 760 K wall temperature for 1.0 mm blunt leading edge. As can be seen, for all cases, the SWBLI near the corner between wedges leads to boundary-layer separation in the first wedge that reattaches on the second wedge. This generates a region of slight pressure increase in the first wedge followed by a more pronounced pressure increase due to the second wedge compression. As can be noticed in these figures, the measurements yield consistent slightly higher values than the calculated ones. Among many possible reasons for that, the authors believe that possible uncertainties in the free stream conditions given in the reference and used in the calculations and/or high temperature effects in the air such as molecular dissociation, which is not considered in the present modeling, might be the most probable reasons. Regardless these small differences between measurements and calculations, both models reproduce well the pressure behavior on the wedges. As can be seen, both models present quite similar results in the entire range, although the k-kl-ω one estimates the boundary-layer separation location a little bit better than the SST model.

By looking at the results in Fig. 6, it can be observed that, for the degree of leading edge bluntness presented here, the separation region gets larger and the pressure rise in the second wedge gets more gradual with the effects of the entropy layer generated by the blunt leading edge. It can be noticed exactly the same trend when the wall temperature is increased from 300 K to 760 K for the blunt leading edge case, which is similar to the findings for the sharp leading edge case (Moura, 2014; Neuenhahn and Olivier, 2006).

Figure 5 and Fig. 6 also show the Stanton number on the double wedges. Neither model presented good results, mainly in the more important region of high heat flux in the second wedge, when compared to the experimental data. Clearly, the k-kl-ω model underpredicts by much whereas, in general, the transition SST model overpredicts the heat flux on the second ramp, although, the latter seems to be a little bit superior. Comparing the experimental results in both figures for sharp and blunt leading edge, it can be seen that the heat flux on the second ramp is reduced by a blunt leading edge.

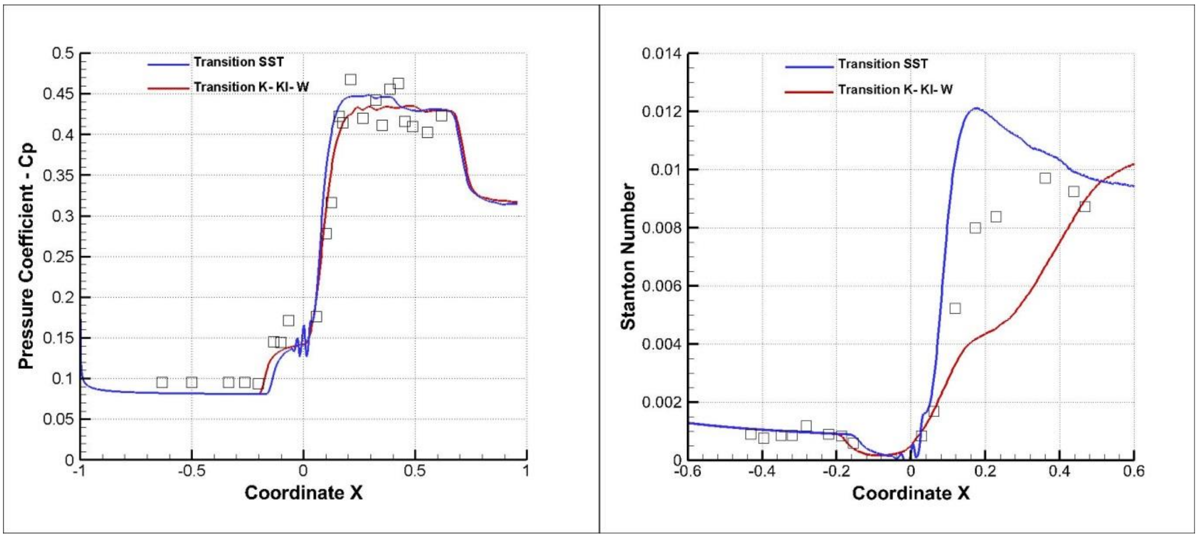

Figure 5. Experimental (symbols) and calculated (lines) pressure coefficient (left) and Stanton number (right), for both transition models, over the double wedge with sharp leading edge and wall temperature of 300K.

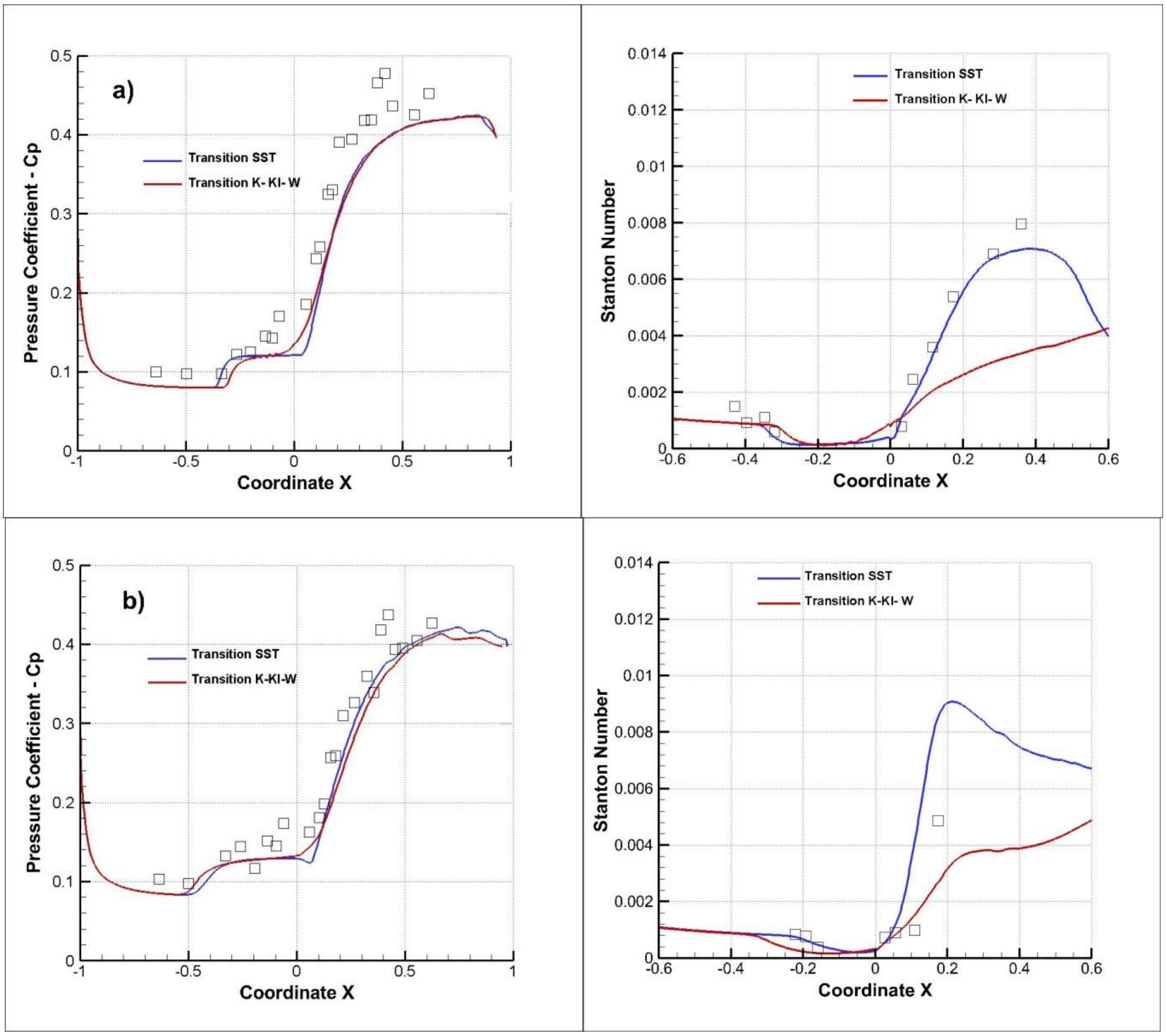

Figure 6. Experimental (symbols) and calculated (lines) ressure coefficient (left) and Stanton number (right), for both transition models, over the double wedge with a) 1.0 mm radius blunt leading edge and 300 K wall temperature, b) 1.0 mm radius blunt leading edge and 760 K wall temperature.

Part 3.3 – 14X-B forebody and compression ramp analysis

The objective in this subsection is to analyze numerically the 14X-B forebody leading-edge-bluntness effects on the airflow in the region bounded by the vehicle forebody and compression ramp of the intake, which has a double wedge configuration whose dimensions, free stream flow and wall thermal conditions are summarized in Tab. 1 and Tab. 2. Figure 7 shows the pressure coefficient on the walls for 300 K (left) and adiabatic (right) wall thermal conditions. Both results were obtained using the transition flow k-kl-ω model. Analyzing the results, for both adiabatic and 300 K wall temperature cases, it was possible to observe that the bigger the radius the lower the slope of the curve of the pressure coefficient on the second wedge. Also, the flow separation bubble in the forebody initially grows and then decreases as the leading edge radius is continuously increased for both wall thermal conditions, which shows that the bubble size reaches a maximum for a certain radius and then diminishes as the radius is further increased, which is in accordance with previous findings (Neuenhahn and Olivier, 2006, Holden, 1971). As can be seen, for the calculations presented in Fig. 7, this maximum occurs for the 1mm-radius leading edge for both wall conditions.

Figure 7 also shows the Stanton number distribution calculated with the transition SST model for different leading edge radii. Regarding the heat flux on the second ramp, it was possible to observe that by increasing the leading edge bluntness the heat flux peak is reduced and moves slightly downstream, which is in conformity with the experimental results by Neuenhahn and Olivier (2006).

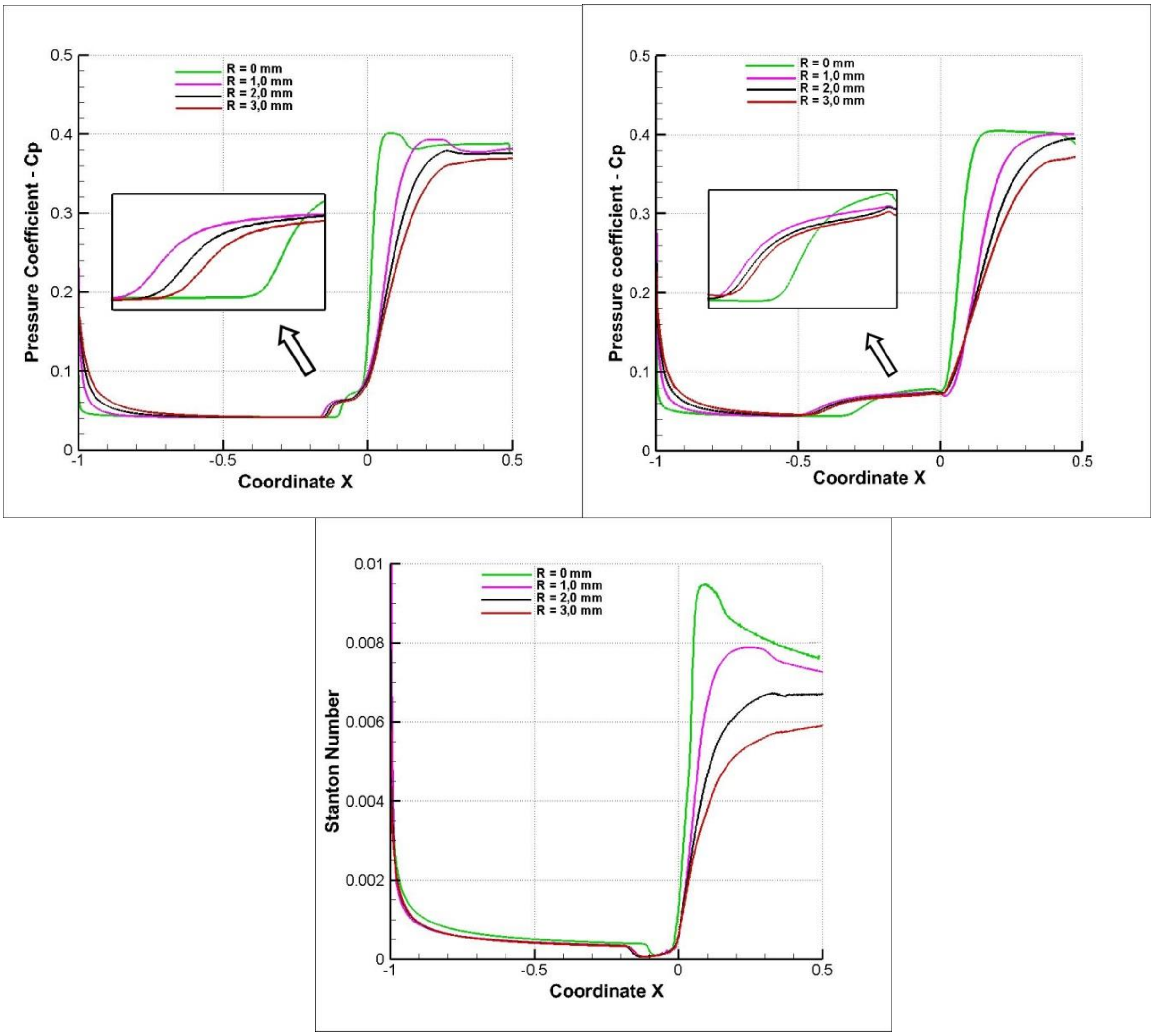

Figure 7. Calculated pressure coefficient with the *k-kl-ω* model on the 14X-B forebody and compression ramp for different leading edge bluntness : 300K wall temperature (left) and adiabatic wall (right). Calculated Stanton Number with the transition SST model and 300 K wall temperature (down).

Figure 8 shows the Mach number contours for sharp and blunt leading edges to illustrate the presence of flow separation near the corner. These results show that leading edge bluntness leads to thicker leading edge shock-wave layer and greater boundary layer separation region.

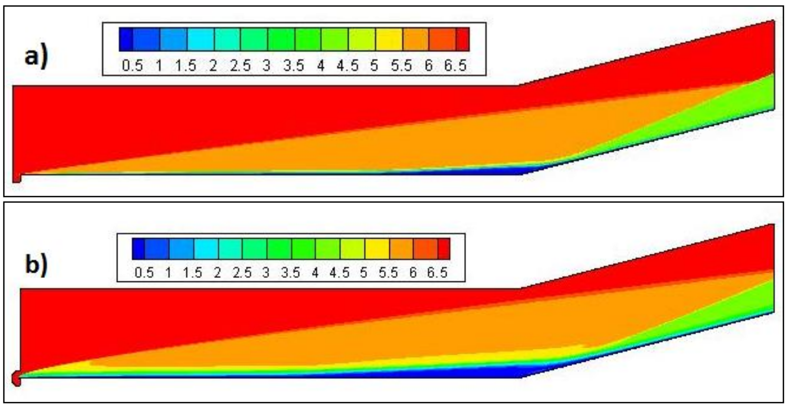

Figure 8. 14X-B forebody and compression ramp Mach number contours for a) sharp leading edge, b) 1.0 mm radius blunt leading edge .

4. CONCLUSIONS

This work presented a numerical analysis of the effects of the 14-XB forebody leading edge bluntness on the airflow structure at the region of the vehicle forebody and the compression ramp. A validation analysis of the transition flow models available in the Fluent code was performed which showed that they are both very reasonable for calculating the pressure on the wall but lack in precision to calculated the high heat flux caused by SWBLI, although the Transition SST model can still capture the right trends.

The results indicate that, regardless the viscous models or wall temperatures, the bubble size present in the corner of the compression ramps due to SWBLI reaches a maximum for a certain radius and then diminishes as the radius is further increased. Calculations show that this maximum occurs for the 1mm-radius leading edge for both wall conditions. This information is in accordance with previous findings (Neuenhahn and Olivier, 2006, Holden, 1971). Analyzing the second ramp, it could be observed that by increasing leading edge bluntness both the heat flux and pressure peaks reduce and move slightly downstream in the second ramp. These airflow changes with leading edge bluntness certainly affect the airflow in the entire intake system, so this is the subject of the next analysis.

5. ACKNOWLEDGEMENTS

The authors would like to acknowledge CNPq for the financial support provided to project number 560143/2010-9.

6. REFERENCES

Anderson, J. D. *Modern Compressible Flow*. 2nd ed. New York: McGraw-Hill,1990. p. 650
Ansys, Fluent 15.0 User's Guide, 2014.
Arnal, D.; Délery, J. Laminar-turbulent transition and shock wave/boundary layer interaction. Critical Technologies for Hypersonic Vehicle Development. Rhode-St-Genèse, Belgium: NATO, 2004
Holden, M.S., "Boundary-Layer Displacement and Leading-Edge Bluntness Effects on Attached and Separated Laminar Boundary Layers in a Compression Corner. Part II: Experimental Study, "AIAA Journal, Vol 9, No 1, 1971, pp. 84-93.
Neuenhahn, T., Olivier, H., 2006. "Influence of The Wall Temperature and the Entropy Layer Effects on Double Wedge Shock Boundary Layers Interactions "14th AIAA/AHI Space Planes Hypersonic Systems and Technologies Conference ". 2006-8136
Menter, F.R., 1994. "*Two-equation eddy-viscosity turbulence models for engineering applications*". AIAA Journal, Vol. 32, No. 8, pp. 1598–1605. ISSN 0001-1452. doi:10.2514/3.12149. URL
Menter, F.R., Langtry, R.B., Likki, S.R., Suzen, Y.B., Huang, P.G. and Volker, S., 2006. "*A Correlation-Based Transition Model Using Local Variables—Part I: Model Formulation*". Journal of Turbomachinery, Vol. 128, No. 3, p. 413. ISSN 0889504X. doi:10.1115/1.2184352. URL http://turbomachinery.asmedigitalcollection.asme.org/article.aspx?articleid=1467239 .
Moura, A.F., 2014. *A computational study of the airflow in scramjet intakes*. Master's thesis, Instituto Tecnológico de Aeronáutica, São José dos Campos, Brazil.
Moura, A.F., Rosa, M. A. P. 2014, A numerical Investigation of scramjet engine air intakes for the 14-X hypersonic vehicle.In 6 th European Conference on Computational Fluid Dynamics, ECFD VI, 2014, Barcelona, Spain.
Reinartz, B. et al. Shock wave/boundary layer interaction in hypersonic intake flows. 2nd European Conference for Aerospace Sciences, p. 1–8, 2007.
Walters, D.K. and Cokljat, D., 2008. "A Three-Equation Eddy-Viscosity Model for Reynolds. Averaged Navier–Stokes Simulations of Transitional Flow". Journal of Fluids Engineering, Vol. 130, No. 12, p. 121401. ISSN 00982202. doi:10.1115/1.2979230. URL http://fluidsengineering.asmedigitalcollection.asme.org/article.aspx?articleid=1478203 .

7. RESPONSIBILITY NOTICE

The authors are the only responsible for the printed material included in this paper.